Electronic Supplementary Information

A durable MXene-based zinc ion hybrid supercapacitor with sulfated polysaccharide reinforced hydrogel/electrolyte

Haonan Cui[a], Hongyu Mi[a,*], Chenchen Ji[a,c,*], Fengjiao Guo[a], Yanna Chen[a], Dandan Wu[a], Jieshan Qiu[b,*], Haijiao Xie[d]

[a] School of Chemical Engineering and Technology, Xinjiang University, Urumqi 830046, People's Republic of China

[b] State Key Laboratory of Chemical Resource Engineering, College of Chemical Engineering, Beijing University of Chemical Technology, Beijing 100029, People's Republic of China

[c] State Key Laboratory of Fine Chemicals, Dalian University of Technology, Dalian 116024, People's Republic of China

[d] Hangzhou Yanqu Information Technology Co., Ltd., Hangzhou 310003, People's Republic of China

*Corresponding author. E-mail: Chenchen Ji, jichenchen2010@163.com; Hongyu Mi, mmihongyu@163.com; Jieshan Qiu, qiujs@mail.buct.edu.cn

1 Experimental section

1.1 Materials

All chemicals were used as received without further purification. MAX phase (Ti_3AlC_2, 200 mesh, 98%) were purchased from Forsman Scientific Co. Ltd. (Beijing, China). Formaldehyde solution (37-40%) were purchased from Xilong Science Co. Ltd. (Guangdong, China). Acrylic acid (99%), Zinc Sulfate (99.5%), κ-carrageenan, and 2-hydroxy-4′-(2-hydroxyethoxy)-2-methylpropiophenone (98%) were purchased

from Shanghai Aladdin Bio-Chem Technology Co. Ltd. (Shanghai, China). Acrylamide (98%), melamine (99.5%) was supplied by Hongyan Chemical Reagent Factory (Tianjin, China). Potassium chloride (99.5%) and N, N′-methylenebisacrylamide (98%) were bought from Baishi Chemical Co. Ltd. (Shanghai, China). Formic acid (88%) was bought from Xi'an Chemical Reagent Factory (Xi'an, China). Hydrochloric acid (37%) was bought from Zhengzhou Xingyang Yellow River Chemical No. 1 Factory (Zhengzhou, China).

1.2 Synthesis of MXene

A minimally intensive layer delamination (MILD) method was used to exfoliate Ti_3AlC_2 (MAX phase) as reported previously.[1] Briefly, 1 g Ti_3AlC_2 powder was slowly added into the pre-prepared 20 mL 9 M HCl aqueous solution contained 1.6 g LiF, which was stirred at 35 ℃ for 12 hours. After standing overnight and further stirring for 12 hours, the obtained suspension was centrifugal washed several times with deionized (DI) water at 3500 rpm until pH value reached to 6. Then the sediment was re-dissolved in 25 mL DI water, followed by exfoliating the MXene flake though hand shaking for 30 min. Finally, the MXene flakes were obtained by collecting the supernatant after centrifuged at 3500 rpm for 30 min.[1]

1.3 Synthesis of MF

Typically, 2.8 g melamine was added into the pre-prepared solution which contains 10 mL formaldehyde and 200 mL DI water. The mixture solution was heated to 80 ℃ under stirring for 30 min to make the solution totally clear. Then 300 μL formic acid was quickly poured into the above solution to accelerate the reaction. After stirring for

1 h, the solution was quickly placed in a cold water to terminate the polyreaction. Then, the cold solution was centrifugal washed at 3500 rpm several times with DI water and ethanol. Finally, the MF was produced by dried overnight at 60 ℃.[2]

1.4 Synthesis of NMXC and NC

Briefly, 800 mg MF was dispersed in 200 mL DI water followed by slowly adding 50 mL MXene ink (2 mg mL^{-1}) to form the dark green precipitation. Then MXene/MF was obtained by centrifugating at 3500 rpm for 5 min and freeze-dried overnight. Finally, 800 mg of the prepared sample were annealed at 550 ℃ under Ar atmosphere with a heating rate of 5 ℃ min^{-1} to get NMXC. The NC was synthesized via the same process without adding any amount of MXene.[2]

1.5 Preparation of PAM-co-PAA/κ-CG hydrogel/electrolyte

PAM-co-PAA/κ-CG hydrogel was synthesized by a one-plot method. Briefly, 4.0 g acrylamide monomer, 2.72 mg N, N′-methylenebisacrylamide crosslinking agent, 0.214 g acrylic acid monomer, 0.132 g UV-initiator (2-hydroxy-4′-(2-hydroxyethoxy)-2-methylpropiophenone), and 0.014 g KCl were gradually added into 16 mL DI water and stirred for 30 min at room temperature. Then 0.240 g κ-CG was slowly added into the above solution and stirred at 350 rpm in 60 ℃ for 1 h. Next, the resulting dispersion was transferred into a glass mold followed by cooling the dispersion at 4 ℃ for 30 min to form a physically crosslinked κ-CG first network. Finally, the PAM-co-PAA/κ-CG hydrogel was obtained by placing the glass mold under UV-irradiation for 1 h. The PAM-co-PAA/κ-CG hydrogel/electrolyte was synthesized by soaking the above hydrogel into 2 M $ZnSO_4$ aqueous solution for 12

h.[3] In order to eliminate the effect of electrolyte thickness in the electrochemical performance, the thicknesses of PAM-co-PAA/κ-CG/$ZnSO_4$ and PAM-co-PAA/$ZnSO_4$ hydrogel/electrolytes in this work were fixed at 1.5 mm for all the tests.

1.6 Electrochemical characterizations

The electrochemical behaviors of pure MXene, NMXC, and NC samples were investigated by CV and EIS measurements on an electrochemical workstation (CHI 660D, Chenhua, Shanghai). The GCD, rate, and cycling performances were revealed by a LAND test system. The specific capacities and energy densities were read out from the above test equipment. The power densities were calculated based on Equation (1):[4]

$$P = \frac{3600E}{t} \tag{1}$$

where E and t represent the voltage window and discharge time, respectively.

1.7 Physical characterizations

To reveal the microstructures of the prepared samples, transmission electron microscopy (TEM, FEI Tecnai G2 F30), the field emission scanning electron microscopy (FESEM, SU-8010), high-resolution transmission electron microscopy (HRTEM), and the corresponding selected area electron diffraction technology (SEAD, FEI Tecnai G2 F30) were employed. X-ray powder diffraction (XRD, Brüker D8) measurements with Cu Kα radiation were used to explored the crystalline structure of the prepared samples. Raman spectra were performed from Micro-Raman spectrometer (Brüker Senterra spectrometer). Nitrogen adsorption/desorption isotherms were conducted at 77 K using the microporous analyzer equipment (3H-

2000PM1/2). X-ray photoelectron spectroscopy spectra (XPS) were recorded from ESCALAB 250Xi instrument to reveal the chemical valence states of the sample. Fourier transform infrared spectra (FTIR) were obtained from VERTEX 70 spectrometer in the range of 550–4000 cm^{-1}. Thermogravimetric analysis (TGA) was performed on TGA55 instrument under an air atmosphere from room temperature to 900 °C with a heating rate of 10 °C min^{-1}. AFM image was collected by using Bruker Dimension Icon under ambient conditions. The contact angles of pure MXene, NMXC, and NC samples were tested on a contact angle testing system (JC2000-CG400).

1.8 Computational methods

All the density functional theory (DFT) calculations were performed on the Vienna Ab Initio Package (VASP) within the generalized gradient approximation (GGA) using the PBE formulation.[5-7] The projected augmented wave (PAW) potentials were employed to describe the ionic cores.[8,9] The valence electrons were revealed by using a plane wave basis set with a kinetic energy cutoff of 500 eV. Partial occupancies of the Kohn−Sham orbitals were allowed using the Gaussian smearing method with a width of 0.05 eV. The self-consistent will be considered for the electronic energy when the energy change was smaller than 10^{-5} eV. A geometry optimization was considered convergent when the force change was smaller than 0.02 eV/Å. Grimme's DFT-D3 methodology was also employed to describe the dispersion interactions.[10]

2. Results and discussion

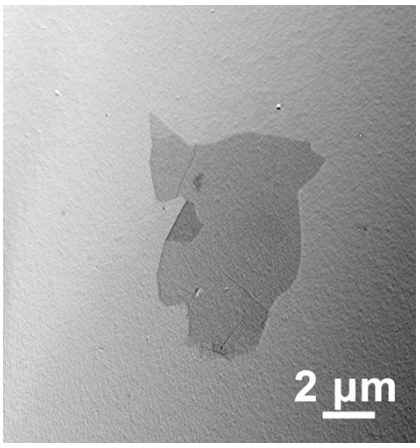

Fig. S1 The TEM image of MXene flake made by MILD method.

Fig. S2 From left to right, the photographs show MXene, MF, and MXene/MF dispersions.

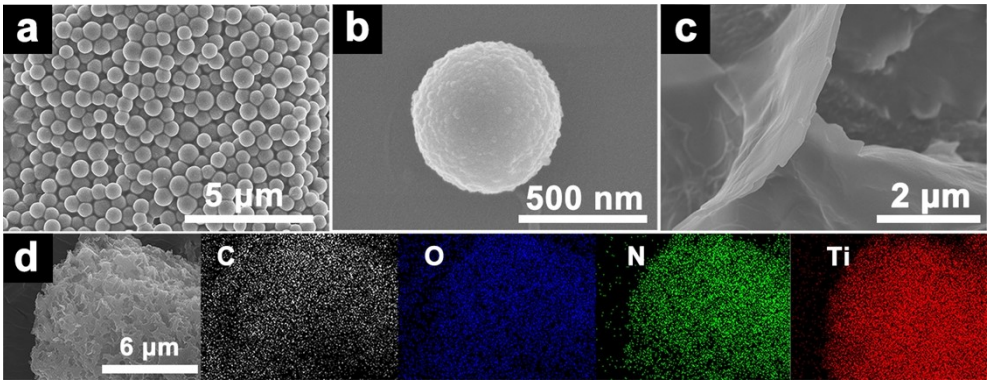

Fig. S3 SEM images of (a) MF, (b) a single MF sphere, and (c) NC. (d) SEM image and the corresponding element mapping images of NMXC.

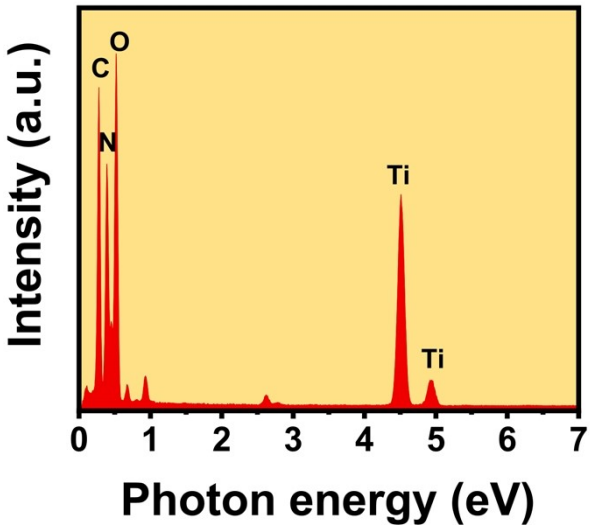

Fig. S4 EDX spectrum of the NMXC sample.

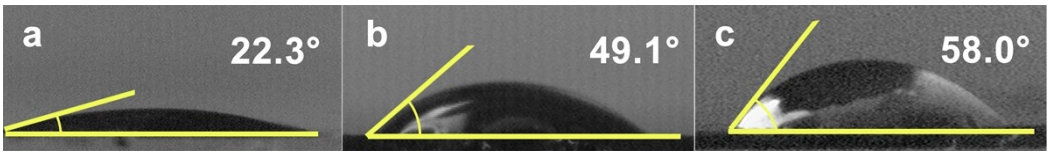

Fig. S5 Water contact angles of (a) pure MXene, (b) NC, and (c) NMXC samples.

The thermogravimetric analysis (TGA) was also performed to reveal the thermal stability of NMXC in air atmosphere. As shown in Fig. S6, the NMXC sample lost up to 5.4% of its weight before 200 ℃, which can be attributed to the removal of the surface functional groups for $Ti_3C_2T_x$ and the loss of water for NMXC [11-13]. The loss of surface functional groups below 200 ℃ may follow the possible reaction Equation (2): [13]

$$Ti_3C_2T_x \rightarrow Ti_3C_2 + T_x \quad (2)$$

The weight increased from 94.6 to 97.1% within 200 ~ 340 ℃ in the TGA curve of the NMXC sample, corresponding to the Ti_3C_2 was partially oxidized to TiO_2 of Equation (3)[13] and the removal of the surface functional groups described in Equation (2).

$$Ti_3C_2 + 3O_2 \rightarrow TiO_2 + 2C \quad (3)$$

The increased weight phenomenon in TGA can be observed in many MXene-based materials.[12-16] After that, the weight decreased 64.1% rapidly after 340 ℃ and maintained at 32.8% after 600 ℃, which can be assigned to the released gas (*e.g.*, CO_2) derived from the completely decomposition of NC and the formed carbon from the thermal conversion reaction of Ti_3C_2 described in Equation (3) under an air

atmosphere.[17-22] Based on the TGA analysis, the content of NC in NMXC was calculated to approximately be 71.6% of the initial weight in the composite.

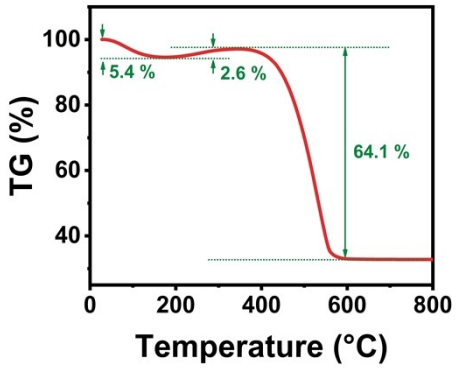

Fig. S6 TGA curve for NMXC in an air atmosphere.

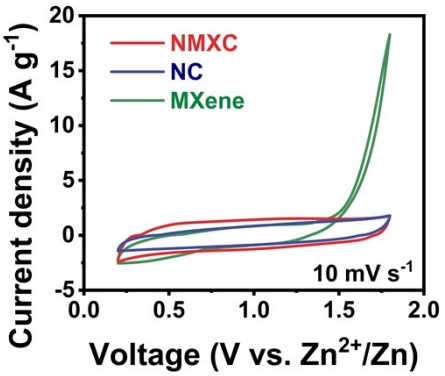

Fig. S7 CV profiles of Zn//MXene, Zn//NC and Zn//NMXC ZHSCs in aqueous $ZnSO_4$ electrolyte within the voltage window of 0.2-1.8 V at 10 mV s^{-1}.

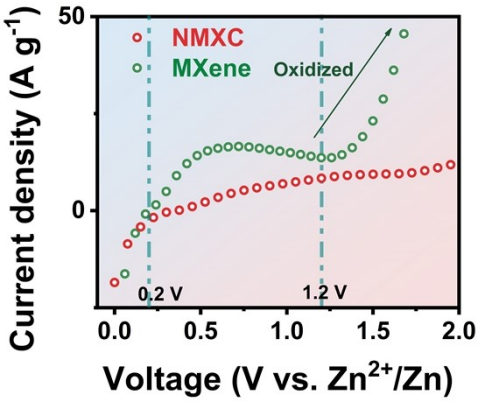

Fig. S8 LSV curves of Zn//MXene and Zn//NMXC ZHSCs in aqueous $ZnSO_4$ electrolyte at 100 mV s^{-1}.

The *ex-situ* XRD spectra were adopted at the selected five states to explore the structural changes of the NMXC cathode and Zn anode in aqueous ZHSC during the electrochemical charge storage process (Fig. S9a). As shown in Fig. S9b, except the characteristic peak of PTFE (JCPDS No. 54-1595) at 17.7°, the peaks of the $Zn_4SO_4(OH)_6{\cdot}4H_2O$ byproduct (JCPDS No. 44-0673) were gradually emerged on

NMXC cathode as the electrochemical charge and discharge proceeds, which may result from the chemical reactions between the OH^-, $ZnSO_4$, and H_2O species.[23] And only slight variation in the intensity without new characteristic peaks appears in the XRD patterns in Fig. S9c for metal Zn (JCPDS No. 04-0813). The above results are in consistent with the reported works.[4,24,25]

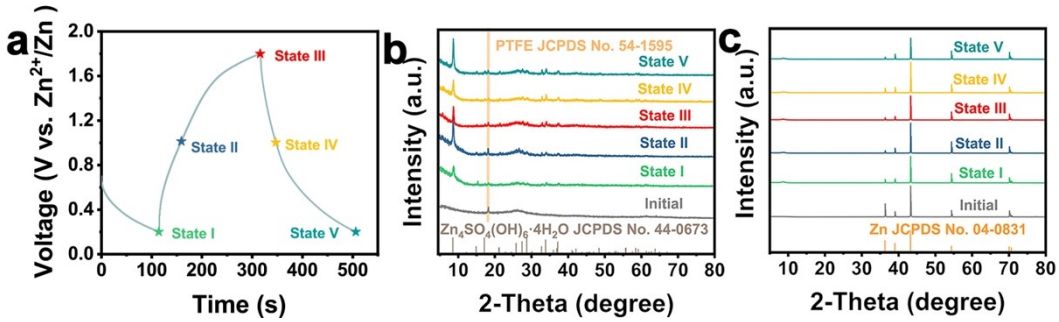

Fig. S9 (a) GCD curve. The *ex-situ* XRD patterns recorded at different charge/discharge states with a current density of 1 A g^{-1} for (b) NMXC cathode and (c) Zn anode.

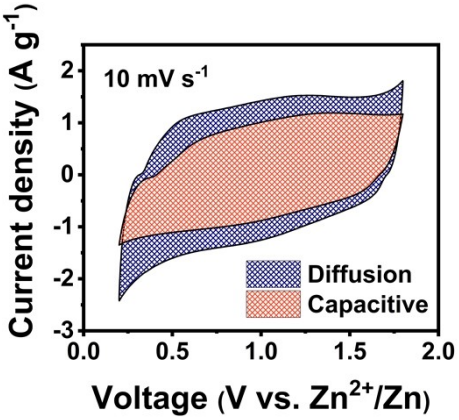

Fig. S10 Capacitive contribution to the total capacity from CV analysis at 10 mV s^{-1}.

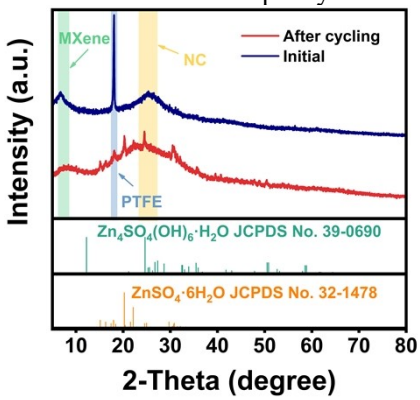

Fig. S11 The *ex-situ* XRD patterns of NMXC electrodes before and after 9000 cycles in 2 M $ZnSO_4$.

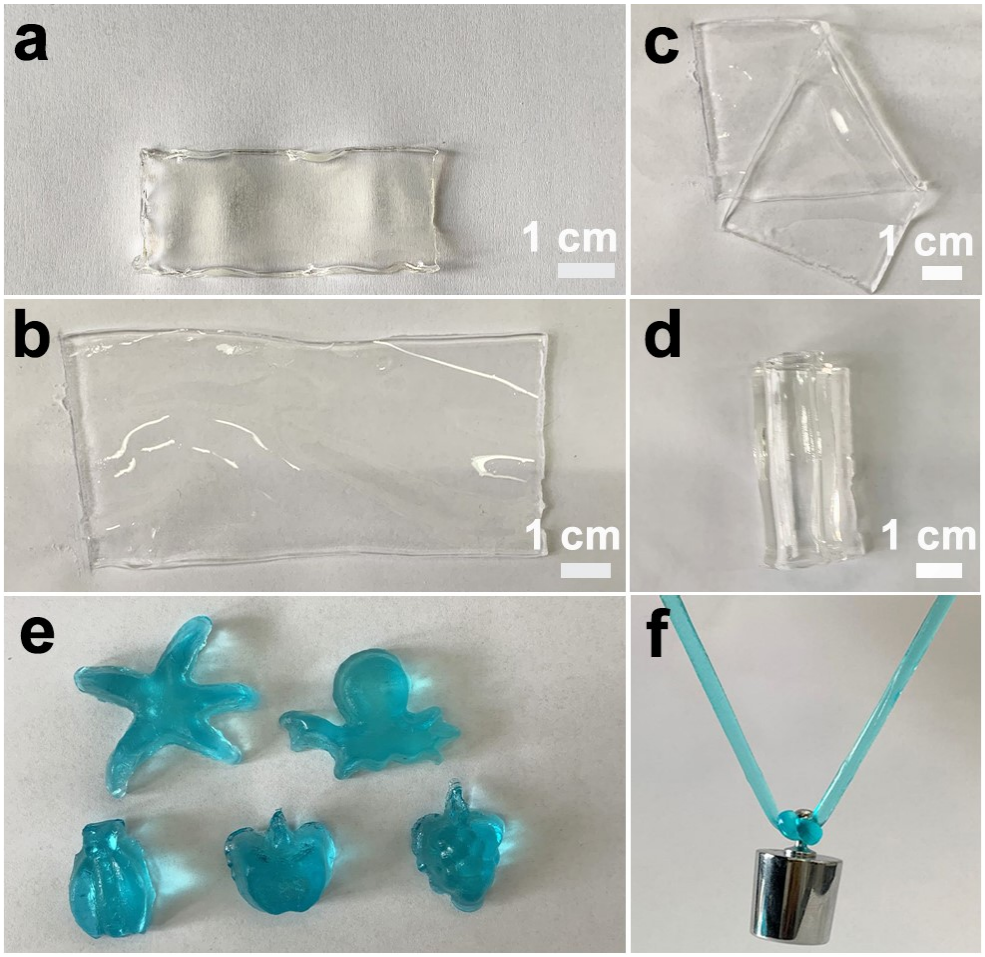

Fig. S12 Digital photos of (a) PAM-co-PAA/κ-CG and (b) PAM-co-PAA/κ-CG/$ZnSO_4$ hydrogels. The PAM-co-PAA/κ-CG/$ZnSO_4$ hydrogel/electrolyte can be easily (c) folded, (d) rolled, (e) molded into complex shapes, and (f) even can hold a weight of 20 g.

Fig. S13 A digital photo of the soft packaged quasi-solid-state ZHSC.

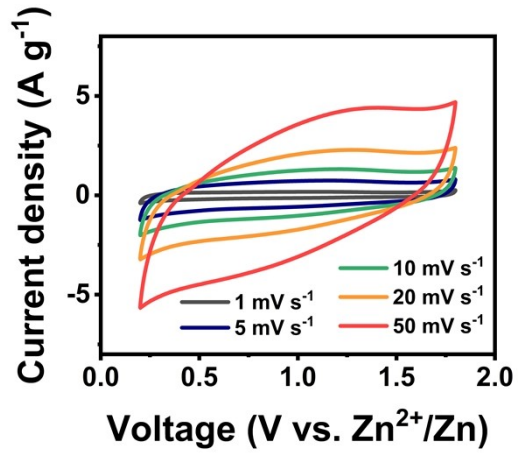

Fig. S14 The CV profiles at various scan rates of the quasi-solid-state ZHSC.

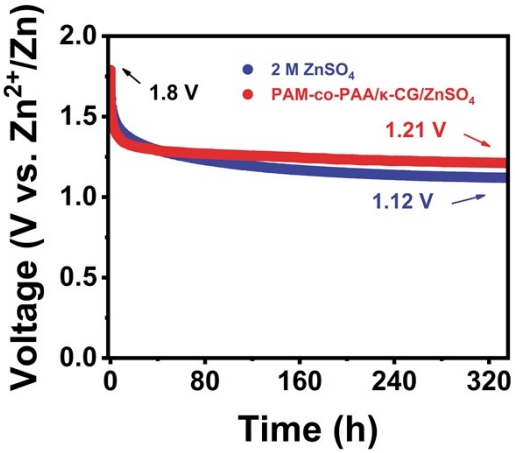

Fig. S15 The self-discharging curves of NMXC based ZHSCs with PAM-co-PAA/κ-CG/$ZnSO_4$ and 2 M $ZnSO_4$ electrolytes.

Notes and references

1 M. Alhabeb, K. Maleski, B. Anasori, P. Lelyukh, L. Clark, S. Sin and Y. Gogosti, *Chem. Mater.*, 2017, **29**,7633-7644.

2 L. Yu, Z. Fan, Y. Shao, Z. Tian, J. Sun and Z. Liu, *Adv. Energy Mater.*, 2019, **9**, 1901839.

3 S. Liu and L. Li, ACS. *Appl. Mater. Interfaces*, 2016, **8**, 29749-29758.

4 J. Huang, L. Wang, Z. Peng, M. Peng, L. Li, X. Tang, Y. Xu, L. Tan, K. Yuan and Y. Chen, *J. Mater. Chem. A*, 2021, **9**, 8435-8443.

5 G. Kresse and J. Furthmüller, *Comput. Mater. Sci.*, 1996, **6**, 15-50.

6 G. Kresse and J. Furthmüller, *Phys. Rev. B*, 1996, **54**, 11169-11186.

7 J. P. Perdew, K. Burke and M. Ernzerhof, *Phys. Rev. Lett.*, 1996, **77**, 3865-3868.

8 G. Kresse and D. Joubert, *Phys. Rev. B*, 1999, **59**, 1758-1775.

9 P. E. Blöchl, *Phys. Rev. B*, 1994, **50**, 17953-17979.

10 S. Grimme, J. Antony, S. Ehrlich and H. Krieg, *J. Chem. Phys.*, 2010, **132**, 154104.

11 A. S. Levitt, M. Alhabeb, C. B. Hatter, A. Sarycheva, G. Dionb and Y. Gogotsi, *J. Mater. Chem. A*, 2019, **7**, 269-277.

12 T. S. Mathis, K. Maleski, A. Goad, A. Sarycheva, M. Anayee, A. C. Foucher, K. Hantanasirisakul, C. E. Shuck, E. A. Stach and Y. Gogotsi, *ACS Nano*, 2021, **15**, 6420-6429.

13 L. Li, X. Liu, J. Wang, Y. Yang, Y. Cao and W. Wang, *Compos. Part A: Appl. Sci. Manuf.*, 2019, **127**, 105649.

14 P. Zhang, R. A. Soomro, Z. Guan, N. Sun and B. Xu, *Energy Stor. Mater.*, 2020, **29**, 163-171.

15 H. Zhang, L. Yang, P. Zhang, C. Lu, D. Sha, B. Yan, W. He, M. Zhou, W. Zhang, L. Pan and Z. Sun, *Adv. Mater.*, 2021, **33**, 2008447.

16 H. Liu, X. Chen, Y. Zheng, D. Zhang, Y. Zhao, C. Wang, C. Pan, C. Liu and C. Shen, *Adv. Funct. Mater.*, 2021, **31**, 2008006.

17 L. Liu, Z. Xie, Q. Deng, X. Hou and Z. Yuan, *J. Mater. Chem. A*, 2017, **5**, 418-425.

18 P. C. P. Watts, P. K. Fearon, W. K. Hsu, N. C. Billingham, H. W. Kroto and D. R. M. Walton, *J. Mater. Chem.*, 2003, **13**, 491-495.

19 B. Li, X. Ge, F. W. T. Goh, T. S. A. Hor, D. Geng, G. Du, Z. Liu, J. Zhang, X. Liu and Y. Zong, *Nanoscale*, 2015, **7**, 1830-1838.

20 J. Baek, M. Lee, J. Kim, J. Lee and S. Jeon, *Carbon*, 2018, **127**, 41-46.

21 H.-K. Lai, Y.-Z. Chou, M.-H. Lee and K.-Y. A. Lin, *Chem. Eng. J.*, 2018, **332**, 717-726.

22 M. Yao, Y. Chen, Z. Wang, C. Shao, J. Dong, Q. Zhang, L. Zhang and X. Zhao, *Chem. Eng. J.*, 2020, **395**, 124057.

23 W. Fan, F. Liu, Y. Liu, Z. Wu, L. Wang, Y. Zhang, Q. Huang, L. Fu and Y. Wu, *Chem. Comm.*, 2020, **56**, 2039-2042.

24 Z. Li, D. Chen, Y. An, C. Chen, L. Wu, Z. Chen, Y. Sun and X. Zhang, *Energy Stor. Mater.,* 2020, **28**, 307-314.

25 K. A. Owusu, X. Pan, R. Yu, L. Qu, Z. Liu, Z. Wang, M. Tahir, W.A. Haider, L. Zhou and L. Mai, *Mater. Today Energy*, 2020, **18**, 100529.